PAPER

NJC
www.rsc.org/njc

Incorporation of luminescent lanthanide complex inside the channels of organically modified mesoporous silica *via* template-ion exchange method

Xianmin Guo,[a] Lianshe Fu,*[ab] Hongjie Zhang,*[a] L. D. Carlos,[b] Chunyun Peng,[a] Junfang Guo,[a] Jiangbo Yu,[a] Ruiping Deng[a] and Lining Sun[a]

[a] *Key Laboratory of Rare Earth Chemistry and Physics, Changchun Institute of Applied Chemistry, Chinese Academy of Sciences, Graduate School of the Chinese Academy of Sciences, Changchun, 130022, P. R. China. E-mail: fu@ciac.jl.cn, hongjie@ciac.jl.cn; Fax: +86 431 5698041; Tel: +86 431 5262135*

[b] *Departamento de Física, CICECO, Universidade de Aveiro, 3810-193 Aveiro, Portugal*

Received (in Montpellier, France) 7th April 2005, Accepted 12th July 2005
First published as an Advance Article on the web 8th August 2005

Luminescent lanthanide complex, $Eu(phen)_2Cl_3 \cdot 2H_2O$ (Euphen, phen = 1,10-phenanthroline) has been incorporated inside the channels of mesoporous silica MCM-41 with its external surface modified by phenyltriethoxysilane ($Ph\text{-}Si(OEt)_3$) *via* a simple template-ion exchange method. The passivation of active groups such as silanols in the external surface ensures that the ion exchange reaction occurs between the surfactant cations and the lanthanide complex ions inside the channels of the modified MCM-41. The passivation result is confirmed by ^{29}Si MAS NMR spectroscopy. FT-IR demonstrates that the cationic surfactants are completely removed. XRD and N_2 adsorption–desorption measurements are employed to characterize the mesostructure of Euphen-Ph-MCM-41. Luminescence and stability studies on the materials of Euphen and Euphen-Ph-MCM-41 show that the resultant hybrid material Euphen-Ph-MCM-41 exhibits the characteristic emission of Eu^{3+} ions under UV irradiation with higher $^5D_0$ luminescence quantum efficiency, longer lifetime and better thermal stability than the corresponding pure complex Euphen. Moreover, the characterization results show that the local symmetry and the first coordination shell of Eu^{3+} ions are changed after the complex ions become incorporated into the MCM-41 channels and that a more symmetric environment is occupied by the Eu^{3+} ions in Euphen-Ph-MCM-41 than in Euphen. There is also a more efficient ligand-to-Eu(III) intramolecular energy transfer process in Euphen-Ph-MCM-41.

DOI: 10.1039/b504707b

Introduction

The sol–gel process is a well-known promising technique for preparing inorganic/organic hybrids due to its mild synthetic conditions, processing versatility and capacity for mixing the inorganic and organic precursor components at the nanometer scale.[1] The resultant inorganic/organic hybrids combine excellent mechanical properties and good thermal- or photo- stabilities.[2–4] When functional active molecules such as optical, electronic, magnetic and biological components are incorporated by embedding or grafting into these kinds of matrices, functional organic/inorganic hybrid nanocomposites will be obtained.[5,6] So far, great progress has been made in the incorporation of luminescent molecules into organic/inorganic hybrid matrices for fundamental spectroscopic studies on luminescent properties and development of optical materials.[7,8]

Luminescent materials are very important in a variety of applications such as display systems and lighting technologies. Lanthanide complexes, in particular, are a useful class of luminophores since they exhibit very efficient emission under ultraviolet excitation through protecting metal ions from vibrational coupling and increasing light absorption cross section by the "antenna effect".[9–11] However, they have so far been excluded from practical applications as tunable solid-state lasers or phosphor devices, essentially due to their poor stabilities under high temperature or moisture conditions and low mechanical strength.[12] In order to circumvent these shortcomings, the lanthanide complexes should be incorporated into inorganic or organic/inorganic matrices by low-temperature soft-chemistry processes, including the sol–gel method and hydrothermal synthesis process. To do this, different strategies can be employed: (1) a simple embedding of preformed lanthanide complexes within sol–gel derived hosts; (2) *in situ* syntheses of lanthanide complexes during formation of the oxide network *e.g.* silica, ormosil or inorganic/polymer matrix; and (3) through hydrolysis and condensation of doubly functional trialkoxysilyl units grafted to the sol–gel host. Indeed, to date, much work has focused on this field and many lanthanide complexes have been incorporated into sol–gel derived silica,[13–16] SiO_2/M_xO_y (M = Zr or Ta),[17] ormosil,[18] and SiO_2/polymer[19] matrices or other solid hosts such as zeolite,[20] layered,[21] mesoporous matrices[22] or nanometer silica spheres.[23] Incorporation of lanthanide complexes into these matrices has improved the photo- and thermal-stabilities of the complexes and avoided the self-quenching due to the concentration effect.

Besides the luminescent hybrid materials mentioned above, interesting approaches are to design the functional hybrid materials hierarchically. Zink *et al.* took advantage of the different chemical and physical properties of the regions in the sol–gel films and developed new strategies to place the active molecules, *e.g.* lanthanide complex luminescent molecules, in desired regions.[24] Corriu *et al.* studied the complexation of Eu^{3+} ions inside the channels of ordered mesoporous silica containing chelating groups derived from 3-chloropropyl group-functionalized SBA-15 and cyclam moieties.[25]

MCM-41, one member of the mesoporous materials family, M41S, contains a hexagonal array of one-dimensional channels of uniform mesopores with a pore diameter of 20–100 Å.[26] This perfect periodic nanostructure renders it an ideal host for incorporation of active molecules and some work has already been devoted on this field.[27] As well known, for the as-synthesized MCM-41, the cationic surfactant ions are organized in the form of a cylindrical micellar structure, with its positive ion interacting with the negatively charged silica pore surfaces through Coulombic forces. The weak Coulombic force can be easily broken and the cationic surfactants are replaced by other cations through ion exchange reaction.[28] For instance, Dai *et al.*[29] delivered molecular imprints inside the mesopores using ion exchange reaction, and Badiei *et al.*[30] reported the modification of mesoporous silica by direct template ion exchange using cobalt complex. Functionalization of ordered mesoporous silica materials by organic molecules and control of the location of the guest species within the host architecture in order to achieve the desired properties have recently received considerable interest and are also a great challenge. Through the passivation of the active sites on the external surface of the mesoporous materials MCM-41[29] or SBA-15,[31] controlled synthesis of CdS nanoparticles inside ordered mesoporous silica using ion exchange reaction has been reported.

To our best knowledge, no lanthanide complex has been incorporated before inside the channels of MCM-41 using an ion exchange method. In this work, the surface active silanols (Si–OH) were passivated by reaction of the as-synthesed MCM-41 (with template) with organosilane and the cationic surfactants were ion-exchanged with lanthanide complex ions. This was confirmed by structural and spectroscopic characterizations. The main objective of this work is to develop a novel preparation method for organic/inorganic hybrid materials doped with lanthanide complexes and to investigate their luminescent properties.

Experimental

Materials

Tetraethoxysilane (TEOS), phenyltriethoxysilane (Ph-Si$(OEt)_3$) cetyltrimethylammonium bromide (CTAB) and 1,10-phenanthroline (phen) were used as received. Absolute ethanol (CH_3CH_2OH), methanol (CH_3OH), chloroform ($CHCl_3$) and dichloromethane (CH_2Cl_2) were dried over molecular sieves prior to use at room temperature (RT). Europium(III) chloride ($EuCl_3 \cdot 6H_2O$) was obtained by reaction of europium oxide (Eu_2O_3, 99.99%) with hydrochloric acid (HCl), followed by evaporation of the excess HCl on a water bath, and was then dissolved in EtOH. The molar concentration of $EuCl_3 \cdot 6H_2O$ was determined by EDTA volumetric method using hexamethylenetetramine ($(CH_2)_6N_4$) as the buffer agent and xylenol as the indicator. Ammonium hydroxide solution ($NH_3 \cdot H_2O$, 28%) was used for modulation of the solution basicity when MCM-41 was prepared. All reagents were of analytic grade and purchased from Beijing Chemical Factory except for Ph-Si$(OEt)_3$ from Aldrich. Distilled water was used throughout the experiments.

Synthesis

The incorporation of lanthanide complex $Eu(phen)_2Cl_3 \cdot 2H_2O$ (designated as Euphen) inside the channels of mesoporous material MCM-41 involved two steps: (1) selective functionalization of the external surfaces of MCM-41 thus leaving the inner wall of the channels intact due to the protecting rule of the surfactant;[32] (2) template-ion exchange with lanthanide complex ions ($[Eu(phen)_2]^{3+}$). In detail, in the first step, the active silanols (Si-OH) on the external surface were passivated by reaction with ethoxy groups of Ph-Si$(OEt)_3$ in $CHCl_3$. In the second step, the surfactant cations (cetyltrimethylammonium-CTA^+) were exchanged by $[Eu(phen)_2]^{3+}$. The protocol for this two-step synthesis is shown in Scheme 1, and the typical preparation process is as follows.

(1) Synthesis of Euphen. Euphen was synthesized according to a method similar to the literature:[33] 1.5858 g (8.00 mmol) of phen was dissolved in 21.0 mL of CH_3CH_2OH. To this solution, 2.00 mmol of $EuCl_3 \cdot 6H_2O$ was added under stirring. The mixture was further stirred at room temperature for 3 h and then left overnight. The resulting precipitate was filtered, washed with CH_3CH_2OH, and dried at 50 °C *in vacuo* for 12 h.

(2) Synthesis of MCM-41 with template (designated as as-synthesized MCM-41). 1.100 g of CTAB was added to 26.0 mL of distilled water and heated under stirring until its complete dissolution, followed by addition of 12.0 mL of concentrated $NH_3 \cdot H_2O$. Then 5.00 mL of TEOS was added dropwise to the above solution under vigorous stirring. The molar composition of TEOS : CTAB : NH_3 : H_2O is 1 : 0.13 : 7.9 : 83.4. The mixture was stirred for a further 4 h at room temperature and then transferred to a Teflon-lined autoclave and heated at 100 °C for 48 h. The resulting precipitate was filtered, washed with copious amounts of water, and dried at 70 °C *in vacuo* for 10 h.

(3) Synthesis of functionalized MCM-41 by Ph-Si$(OEt)_3$ (designated as Ph-MCM-41). 0.800 g of as-synthesized MCM-41 was added to a mixed solution of 16.0 mL of Ph-Si$(OEt)_3$ and 64.0 mL of $CHCl_3$. The slurry was refluxed at 35 °C in nitrogen (N_2) atmosphere for 10 h. The resulting product was recovered by filtration, washed with $CHCl_3$ and CH_2Cl_2 respectively four times in order to remove the remaining Ph-Si$(OEt)_3$, and dried at 60 °C *in vacuo* for 10 h.

(4) Synthesis of Ph-MCM-41 without template (named as DPh-MCM-41). Into a 100 mL round-bottom flask, 0.2179 g of Ph-MCM-41 was mixed with 0.31 mL of concentrated HCl and 18.0 mL of CH_3CH_2OH (corresponding to 0.20 mol L^{-1} HCl). The mixture was refluxed at 80 °C for 12 h. The resulting product was recovered by filtration, washed with CH_3CH_2OH four times, and dried at 60 °C *in vacuo* for 10 h.

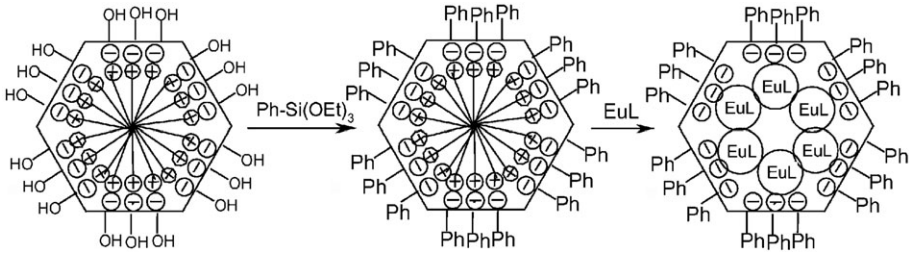

Scheme 1 Schematic diagram of incorporation of lanthanide complex into the channels of functionalized mesoporous material MCM-41 with L = phen, the charge in Euphen was omitted for simplification.

(5) Synthesis of functionalized MCM-41 containing Euphen inside the channels (designated as Euphen-Ph-MCM-41). 0.7339 g (1.11 mmol) of Euphen was added to 0.3416 g of Ph-MCM-41 in 16.0 mL of CH_3OH. The mixture was stirred at room temperature for 10 h. The resulting product was filtered, washed with CH_3OH four times, and dried at 60 °C *in vacuo* for 10 h.

Characterization

The powder X-Ray diffraction (XRD) patterns were recorded in the 2θ range of 0.50 to 10.0° with a Rigaku-D/Max 2500 diffractometer using Cu Kα radiation ($\lambda = 1.5418$ Å) at 40 kV and 200 mA.

Fourier transform infrared spectra (FT-IR) were measured with a Bruker Vertex 70 spectrophotometer within the wavenumber range 4000–400 cm^{-1} using KBr pressed pellet technique.

Solid-state ^{29}Si magic-angle spinning (MAS) NMR spectra were recorded at 79.46 MHz using a Bruker Avance 400 spectrometer. The chemical shifts were quoted in ppm from tetramethylsilane (TMS).

N_2 adsorption–desorption isotherms were measured at liquid nitrogen temperature (77 K) using a Nova l000 analyzer. Samples were degassed at 120 °C overnight before measurements. Specific surface areas were calculated using the Brunauer–Emmett–Teller (BET) model and pore size distributions were evaluated from the desorption branches of the nitrogen isotherms using the Barrett–Joyner–Halenda (BJH) model. Pore volumes were estimated at a relative pressure of 0.98 (P/P_0), assuming full surface saturation with nitrogen.

Diffuse reflection UV-Visible (DR UV-Vis) spectra were acquired from Hitachi F-4100 with tungsten and deuterium lamps.

The content of Eu^{3+} in samples was carried out using ICP-AES method on a TJA POEMS ICP atomic emission spectrometer.

TG analysis was performed on an SDT 2960 analyzer (Shimadzu, Japan) from 40 to 800 °C at a heating speed of 10 °C per min under air atmosphere.

The excitation and emission spectra were carried out at room temperature with a Hitachi F-4500 spectrophotometer equipped with a 150 W Xenon lamp as the excitation source. Luminescence lifetimes were measured with a Lecroy Wave Runner 6100 digital oscilloscope (1 GHz) using laser radiation (pulse width = 4 ns) as the excitation source (Continuum Sunlite OPO).

Results and discussion

XRD patterns

The XRD patterns for the as-synthesized MCM-41, Ph-MCM-41 and Euphen-Ph-MCM-41 are shown in Fig. 1. The patterns for as-synthesized MCM-41 and Ph-MCM-41 display four well-defined peaks in the 2θ range of 2–6° with *d* spacings of *ca*. 40, 24, 20 and 15 Å. The well-resolved peaks with the *d*-value ratio of $1:1/\sqrt{3}:1/2:1/\sqrt{7}$ can be indexed as (100), (110), (200) and (210) reflections of a highly ordered hexagonal mesostructure, respectively.[26] The pattern for Euphen-Ph-MCM-41 presents three well-resolved peaks with *d* spacings of 41, 24 and 20 Å, which are similarly indexed as (100), (110) and (200) reflections of hexagonal mesostructure. However, the peak intensity for Euphen-Ph-MCM-41 in XRD pattern decreases after Euphen was incorporated into the channels of Ph-MCM-41. The decrease of peak intensity and nearly disappearance of the reflection (210) in the XRD pattern of Euphen-Ph-MCM-41 suggest that the guest ions in the channels distribute randomly, which would reduce the periodicity, and that the mesoporous structure partially collapses after ion exchange of the template by the Euphen complex ions, which is probably caused by the high content of lanthanide complex through formation of macropores in the solid. Compared to the modified MCM-41, all peaks shifted slightly to higher angles when the surfactant molecules were exchanged by the Euphen complex ions. A similar phenomenon has also been observed in other work.[29a] This is probably because the siloxane polycondensation was not complete, which led to a contraction of the silicious network during the ion exchange process. The hexagonal unit cell parameter, a_0 (the internal pore diameter plus one pore wall thickness) can be calculated according to the formula $a_0 = 2d_{100}/\sqrt{3}$, where d_{100} is obtained from 2θ angle of the first reflection peak in the XRD pattern by Bragg's equation: $2d_{100} \sin\theta = \lambda$ ($\lambda = 1.5418$ Å for the Cu Kα line). The values of d_{100} and a_0 for the materials at different stages during the preparation process are listed in Table 1. As it can be seen, the a_0 value for Euphen-Ph-MCM-41 is slightly smaller than that of Ph-MCM-41 and larger than that of as-synthesized MCM-41, the same result being published previously.[29a]

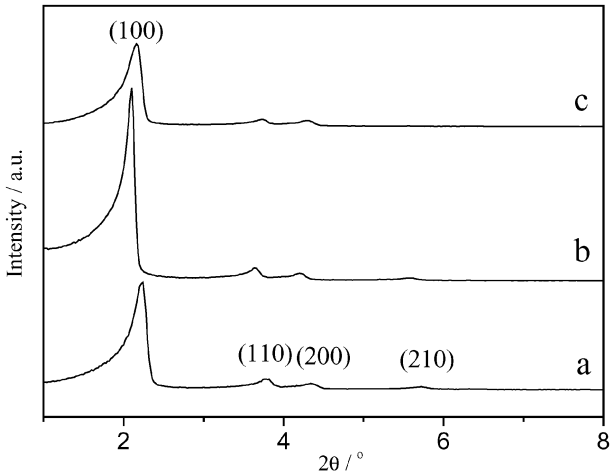

Fig. 1 XRD patterns for as-synthesized MCM-41 (a), Ph-MCM-41 (b) and Euphen-Ph-MCM-41 (c).

Nitrogen adsorption measurements

The N_2 adsorption–desorption isotherm and pore size distribution for Euphen-Ph-MCM-41 (a) and DPh-MCM-41 (b) are shown in Fig. 2. They all exhibit Type IV isotherms with H_1-type hysteresis loops at low relative pressure, which is related to the capillary condensation of nitrogen within the pores. This is characteristic of mesoporous materials according to the IUPAC classification.[34] From the two branches of adsorption–desorption isotherms, the presence of a sharp adsorption step in the P/P_0 region 0.2 to 0.4 shows that all solids possess a well-defined array of regular mesopores. The specific area and the pore size are calculated by the BET method and BJH model, respectively. Samples display a narrow pore size distribution. The values of estimated pore size (PS), pore volume (PV) and BET surface area (SA) are also summarized in Table 1. It can be clearly seen that the SA, PV and PS decrease from 1262 $m^3\ g^{-1}$, 1.36 $cm^3\ g^{-1}$ and 27.9 Å for template-free sample DPh-MCM-41 to 1027 $m^3\ g^{-1}$, 1.02 $cm^3\ g^{-1}$ and 25.6 Å for Euphen-Ph-MCM-41, respectively. This is simply due to the presence of the organic complex in the channels of Ph-MCM-41, as was also observed in the literature.[35]

Solid-state ^{29}Si MAS NMR spectra

The solid-state ^{29}Si MAS NMR spectra for the as-synthesized MCM-41 and Ph-MCM-41 are shown in Fig. 3. The spectrum for the as-synthesized MCM-41 mesoporous solid reveals three

Table 1 Structural parameters of as-synthesized MCM-41, Ph-MCM-41, Euphen-Ph-MCM-41 and DPh-MCM-41

Samples	d_{100}/Å	$a_0{}^a$/Å	PS^b/Å	PV/cm^3 g^{-1}	SA/m^2 g^{-1}
MCM-41	39.6	45.7			
Ph-MCM-41	42.1	48.6			
Euphen-Ph-MCM-41	40.9	47.2	25.6	1.02	1027
DPh-MCM-41	42.6	49.1	27.9	1.36	1262

^{a} Calculated using the equation $a_0 = 2d_{100}/\sqrt{3}$. ^{b} Pore size distribution by desorption branch (BJH).

signals at −110.9, −100.9 and −92.7 ppm, corresponding to (≡SiO)$_4$**Si** (Q^4, siloxane), (≡SiO)$_3$**Si**OH (Q^3, single silanol) and (≡SiO)$_2$**Si**(OH)$_2$ (Q^2, geminal silanol) environments of silicon atoms, respectively.[36] For the spectrum of Ph-MCM-41, the very strong resonances at −110.6 and −101.2 ppm represent silicon atoms in positions Q^4 and Q^3, respectively, while the very weak shoulder appearing at around −96 ppm is assigned to Q^2. The resonance at *ca.* −70 ppm in the spectrum of Ph-MCM-41 is due to the organosiloxane atom (≡SiO)$_3$**Si**R (T^3). The appearance of T^3 functionalities indicates the existence of a covalent linkage between the organic group and the silica surface. In order to study in detail the as-synthesized and Ph-Si(OEt)$_3$-functionalized MCM-41, the spectral deconvolutions are carried out using the ORIGIN® package. The relative concentrations (integrate areas) of all silicon sites are obtained from the deconvolution results. The ratio of $Q^2 + Q^3$ to Q^4 ($(Q^2 + Q^3)/Q^4$) indicates the degree of polycondensation. The external surface coverage (ESC) by organic moieties can be estimated from ESC = $\sum T/\sum Q = T^3/(Q^2 + Q^3 + Q^4 + T^2 + T^3)$, which can allow the quantitative assessment of the modification degree of the organic moiety.[37] The chemical shifts, relative concentration, the value of $(Q^2 + Q^3)/Q^4$ ratio and ESC are summarized in Table 2. As expected, the modification process results in the decrease of the intensities Q^2 and Q^3 and the increase of the intensity of Q^4, *i.e.* the relative concentration of Q^4 increases by 10.5% from MCM-41 to Ph-MCM-41, indicating that some silanols still continue to condense during the modification process, which is well in agreement with the result obtained from XRD patterns. The relative lower value of ESC is due to the fact that the modification reaction took place only on the external surface whereas the inner surface was protected by the surfactant from reaction with Ph-Si(OEt)$_3$.

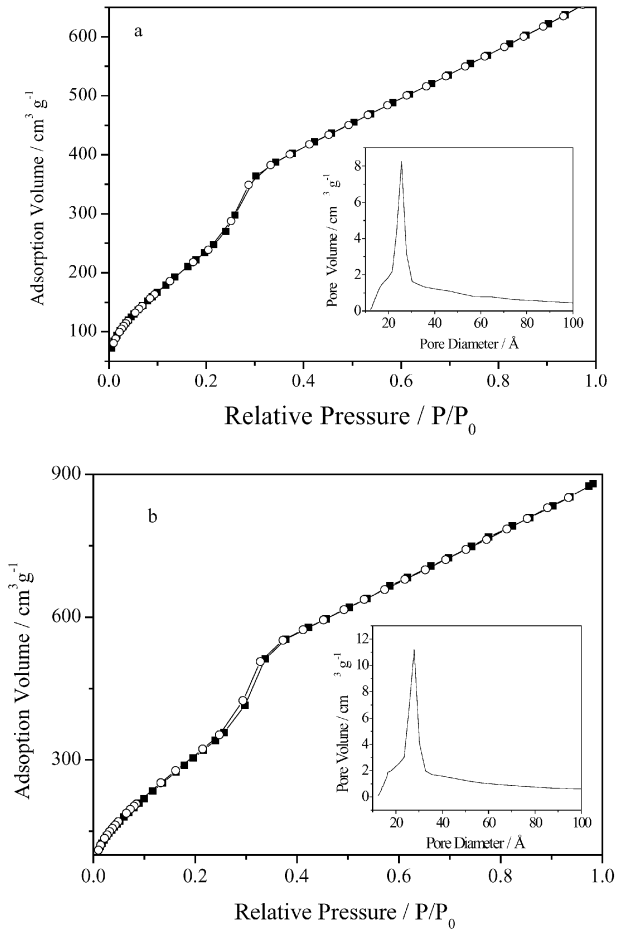

Fig. 2 Nitrogen adsorption–desorption isotherms of Euphen-Ph-MCM-41 (a) and DPh-MCM-41 (b). The corresponding BJH pore distributions are shown in the insets.

FT-IR spectra

The FT-IR spectra of as-synthesized MCM-41, Ph-MCM-41 and Euphen-Ph-MCM-41 are shown in Fig. 4. The evident peaks appearing at 2958 cm^{-1} and 2854 cm^{-1} are due to the asymmetric stretching vibrations of –CH$_3$ and –CH$_2$ aliphatic moieties of the surfactant cations,[38] while the broad bands centered at *ca.* 1480 cm^{-1} are arising from –CH$_3$ deformation and –CH$_2$ scissoring vibrations. These absorption bands have totally disappeared upon template-ion exchange reaction with Euphen complex ions, indicating that the template removal and incorporation of lanthanide complex ions inside the channels of the mesoporous materials occur simultaneously. The broad band peaking around 3390 cm^{-1} corresponds to mainly water molecules adsorbed onto or maybe inside channels; its intensity for Euphen-Ph-MCM-41 is particularly large, which indicates that some water molecules still exist in Euphen-Ph-MCM-41 even after heat treatment at 393 K, since they are adsorbed and rapidly coordinated to Eu^{3+} ions in air. Bands at *ca.* 1068 cm^{-1} and 1232 cm^{-1} for as-synthesized MCM-41 and Ph-MCM-41 are assigned to the asymmetric Si–O–Si stretching vibrations and around 800 cm^{-1} allocated to symmetric Si–O–Si stretching vibrations. The former band undergoes a blue shift from 1068 to 1080 cm^{-1} for Euphen-Ph-MCM-41, suggesting the change of microchemical circumstance of silicon atoms. Moreover, the latter becomes less obvious and almost

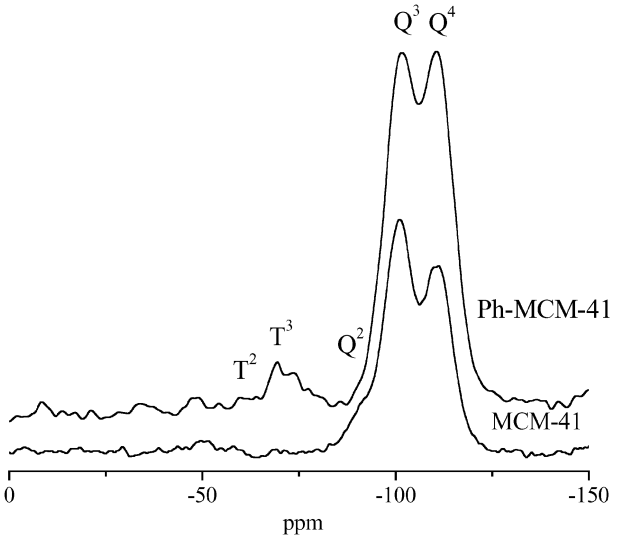

Fig. 3 Solid-state ^{29}Si MAS NMR spectra for as-synthesized MCM-41 and Ph-MCM-41.

Table 2 Chemical shifts, relative concentrations (RC) of T^m and Q^n groups, $(Q^2 + Q^3)/Q^4$ ratios and ESC for MCM-41 and Ph-MCM-41

Samples	Chemical shifts/ppm (RC/%)					$(Q^2 + Q^3)/Q^4$	ESC[a]
	T^2	T^3	Q^2	Q^3	Q^4		
MCM-41			−92.7/12.5	−100.9/43.3	−110.9/44.2	1.26	
Ph-MCM-41		−69.4/6.1	−96.2/9.7	−101.2/29.5	−110.6/54.7	0.72	6.1

[a] Calculated using by the equation ESC = $\sum T/\sum Q = T^3/(Q^2 + Q^3 + Q^4 + T^2 + T^3)$.

forms a wide band with the *ca.* 1068 cm^{-1} band after incorporation of Euphen in the channels. Bands at *ca.* 460 cm^{-1} are attributed to Si–O–Si symmetric bending vibrations. The band at 965 cm^{-1} is associated with silanol (Si–OH) stretching vibrations. In order to study the degree of modification, deconvolutions are calculated from 1290 cm^{-1} to 870 cm^{-1} for as-synthesized MCM-41 and Ph-MCM-41, and the relative intensities of Si–O–Si and Si–OH can be acquired from the deconvolution results. The intensity ratio of Si–OH to Si–O–Si decreases nearly by 50 percent from 0.12 for MCM-41 to 0.056 for Ph-MCM-41, which is similar to the result of $(Q^2 + Q^3)/Q^4$ value change from MCM-41 to Ph-MCM-41 in solid-state ^{29}Si MAS NMR spectra, suggesting that some remaining silanols still polycondense during the functionalization process. The absorption bands corresponding to Euphen were not clearly shown in the spectrum, perhaps because of the lower concentration of Euphen in the hybrid material or the shielding of Euphen vibrations by the surrounding host. A similar phenomenon was also observed in other work.[22d]

Thermal stability

Thermogravimetric analyses of pure complex Euphen and Euphen-Ph-MCM-41 samples were carried out in air from 40 to 800 °C. These are shown in Fig. 5, including the weight loss (TGA) and derivative weight loss (DrTGA) curves. Euphen-Ph-MCM-41 sample exhibits a weight loss of about 4.4% below 175 °C due to the desorption of adsorbed water or other solvent on the material surface. This is followed by a weight loss of *ca.* 11.8% between 175 and 430 °C, corresponding to the decomposition of the organic components of the mesoporous pore wall material.[39] At higher temperature (500–650 °C), a weight loss of about 13.0% is observed, which results from the organic decomposition of Euphen complex in the channels of the modified MCM-41. However, for the weight loss curve of the pure complex Euphen, the dominant decomposition of organic ligands occurs in the temperature region of 290 to 520 °C, which can be seen more obviously from DrTGA curve, indicating that the stability of the template-ion exchanged product has been improved compared to the corresponding pure complex. In addition, compared to the analogous luminescent hybrids obtained by covalently grafting europium complex to the silica network, this hybrid material seems to show higher stability.[22f]

DR UV-Vis absorption spectra

Fig. 6 shows the DR UV-Vis absorption spectra for the pure complex Euphen and the template-ion exchanged product Euphen-Ph-MCM-41. The two curves exhibit a broad band from 200 to 400 nm. The spectrum of the pure complex Euphen displays the maximum peak at 330 nm with a shoulder located at around 268 nm, while the spectrum of Euphen-Ph-MCM-41 presents a maximum peak at 304 nm together with the same shoulder at *ca.* 268 nm. These almost completely overlapped absorption bands could be assigned to $n \rightarrow \pi^*(S_1)$ and $\pi(S_0) \rightarrow \pi^*(S_1)$ transitions of the phen ring. It should be noted that there are also some weaker peaks at 395, 465 and 535 nm appearing in the spectrum of Euphen, which are due to the excitation transitions $^7F_0 \rightarrow {}^5L_6$, $^7F_0 \rightarrow {}^5D_2$ and $^7F_0 \rightarrow {}^5D_1$, respectively. Due to the weaker intensity of $^7F_0 \rightarrow {}^5D_3$, it can be conjectured that this peak was masked by the noise. This result is well in agreement with the result from the photoluminescence excitation spectra, and will be discussed later. The adsorption band of Euphen-Ph-MCM-41 shows a blue shift compared to that of Euphen, implying that the S_1 state shifts to a higher energy state. A parallel phenomenon was attained by other previous reports,[22] the reason for which is probably due to the hypsochromic effect resulting from the polar change of the surrounding environment after the Euphen complex was incorporated into the pore channels of the modified MCM-41.

Photoluminescence characterization

The excitation and emission spectra for the pure complex Euphen and Euphen-Ph-MCM-41 are presented in Fig. 7. The excitation spectra at room temperature were obtained by monitoring the most intense emission wavelength of Eu^{3+} ions at 613 nm. For both excitation spectra, broad bands are exhibited ranging from 200 to 400 nm and attributed to electronic transitions from the ground state level $(\pi)S_0$ to the excited level $(\pi^*)S_1$ of the organic ligand phen. The excitation

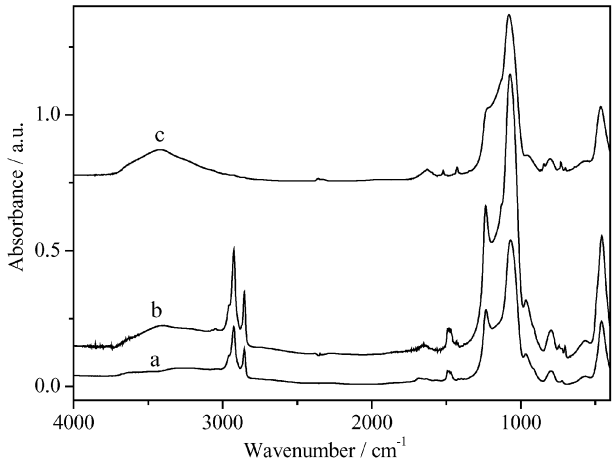

Fig. 4 FT-IR spectra of as-synthesized MCM-41 (a), Ph-MCM-41 (b), and Euphen-Ph-MCM-41 (c).

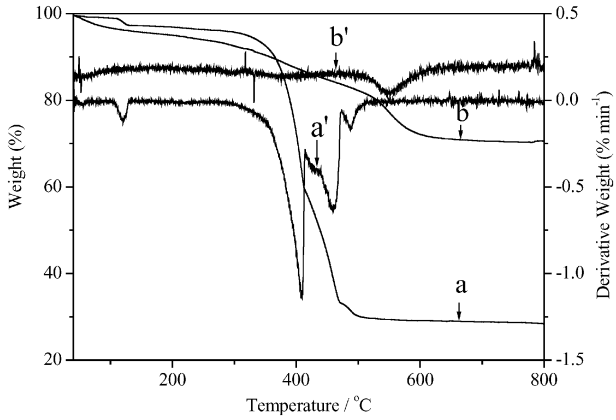

Fig. 5 TGA and derivative TG curves of Euphen (a and a′, respectively) and Euphen-Ph-MCM-41 (b and b′, respectively).

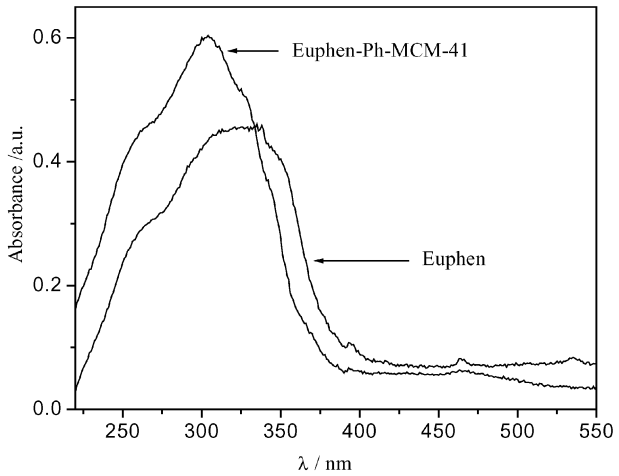

Fig. 6 DR UV-Vis spectra for Euphen and for Euphen-Ph-MCM-41.

spectrum for Euphen displays a distinct band at 336 nm and a shoulder located at around 275 nm, while the excitation spectrum for Euphen-Ph-MCM-41 presents the maximum band at *ca.* 280 nm. In addition, for Euphen, the excitation spectrum also shows some weak sharp peaks at 398 and 468 nm, respectively, assigned to $^7F_0 \rightarrow {}^5L_6$ and $^7F_0 \rightarrow {}^5D_2$ within the measurement range, which are characteristic of absorption line of Eu^{3+} ions, while the weak line near 420 nm probably corresponds to the $^7F_1 \rightarrow {}^5D_3$ excitation band. However, these small sharp peaks almost vanish in Euphen-Ph-MCM-41 excitation spectrum. The emission spectra were obtained by irradiation of samples using the maximum excitation wavelengths 334 nm and 295 nm for Euphen and Euphen-Ph-MCM-41, respectively. They all exhibit the characteristic emission bands at *ca.* 579, 592, 613, 650 and 698 nm corresponding to $^5D_0 \rightarrow {}^7F_J$ ($J = 0$–4), respectively, with the $^5D_0 \rightarrow {}^7F_2$ emission as the dominant band, so-called "europium red" luminescence. From the emission spectrum of Euphen, besides $^5D_0 \rightarrow {}^7F_J$ transitions, two weak bands at 535 and 555 nm are also observed, which are tentatively assigned to the transitions $^5D_1 \rightarrow {}^7F_1$ and $^5D_1 \rightarrow {}^7F_2$, respectively. These two peaks decrease greatly and become very weak in Euphen-Ph-MCM-41 emission spectrum, indicating a more efficient non-radiative relaxation to the $^5D_0$ level when the complex was incorporated in MCM-41 framework.

The $^5D_0 \rightarrow {}^7F_2$ transition is a typical electric dipole transition and strongly varies with the local symmetry of Eu^{3+} ions, while the $^5D_0 \rightarrow {}^7F_1$ transition corresponds to a parity-allowed magnetic dipole transition, which is practically independent of the host material. Therefore, the intensity ratio (R) of $^5D_0 \rightarrow {}^7F_2$ to $^5D_0 \rightarrow {}^7F_1$ is sensitive to the symmetry around Eu^{3+} ions and gives valuable information about environment change.[40] When the R value is higher, the Eu^{3+} ions occupy sites of lower symmetry without inversion center (more asymmetric local environment). However, this ratio is also influenced by other factors like the polarizability of the ligands.[41] The values found decrease from 4.6 for Euphen to 3.4 for Euphen-Ph-MCM-41. This fact suggests that the local symmetry changed as the complex was incorporated into the channels of MCM-41 and indicates a more symmetric environment occupied by the Eu^{3+} ions in Euphen-Ph-MCM-41 than in Euphen, probably due to the effect of confinement. Compared to the pure complex, the emission lines for Euphen-Ph-MCM-41 are wider. This is probably because the local environment of Eu^{3+} ions was changed. The different coordination environments of the central Eu^{3+} ions due to their unsaturated coordination number lead to the wider emission lines of Euphen-Ph-MCM-41. A similar result has been obtained before.[42]

The luminescence decay curves of Eu^{3+} ions related to the $^5D_0 \rightarrow {}^7F_2$ emission are shown in Fig. 8. The decay curves for both Euphen-Ph-MCM-41 and the corresponding pure complex Euphen are singly exponential, confirming that all Eu^{3+} ions lie in the same average environment. The luminescence lifetime was determined to be 0.52 ms and 0.38 ms for Euphen-Ph-MCM-41 and Euphen, respectively. The longer lifetime of Eu^{3+} ions in Euphen-Ph-MCM-41 in comparison with that of Euphen suggests that there is another surrounding for the Eu^{3+} ions, which corresponds to the R value modification. This also corresponds to the decrease in the amount of water near the Eu^{3+} ions.

In order to further discuss these features, the lanthanide luminescence quantum efficiency q and the number of water molecules n_w coordinated to the Eu^{3+} ions in the Euphen-Ph-MCM-41 and Euphen were calculated. The quantum efficiency q is defined by the competition between k_{nr} and k_r processes:

$$q = \frac{k_r}{k_r + k_{nr}} \quad (1)$$

where k_r and k_{nr} denote the radiative and non-radiative probability constants, respectively.

According to Horrocks,[43] n_w can be estimated from the experimental decay time by the empirical formula:

$$n_w = 1.1(k_{exp} - k_r - 0.31) \quad (2)$$

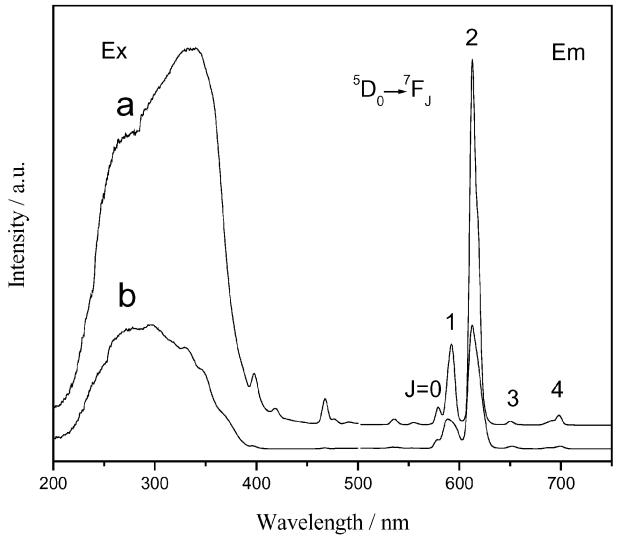

Fig. 7 Excitation and emission spectra for Euphen (a) and for Euphen-Ph-MCM-41 (b) at room temperature.

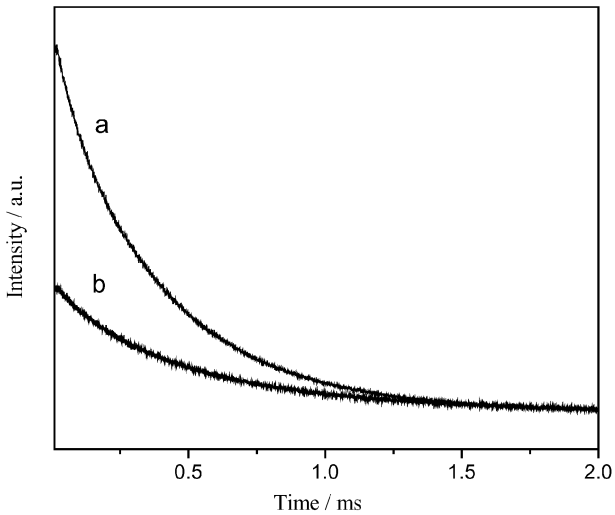

Fig. 8 $^5D_0$ fluorescence decay curves of Euphen (a) and Euphen-Ph-MCM-41 (b) at room temperature.

Table 3 Experimental (k_{exp}) and calculated radiative (k_r) and non-radiative (k_{nr}) $^5D_0$ decay rates (ms^{-1}), decay time (τ, ms), quantum efficiency (q) and number of water molecules coordinated to Eu^{3+} ions (n_w)

Samples	Euphen-Ph-MCM-41	Euphen
τ/ms	0.52	0.38
k_{exp}/ms^{-1}	1.92	2.63
k_r/ms^{-1}	0.41	0.19
k_{nr}/ms^{-1}	1.51	2.44
q/%	21	7
$n_w/\pm0.1$	1.3	2.3

$$k_{exp} = \tau_{exp}^{-1} = k_r + k_{nr} \quad (3)$$

The radiative contribution, k_r, can be calculated from the relative intensities of the $^5D_0 \rightarrow {}^7F_J$ ($J = 0$–4) transitions, and it can be expressed as:[44]

$$k_r = (A_{0-1}E_{0-1}/S_{0-1})\sum_{j=0}^{4}(S_{0-J}/E_{0-J}) \quad (4)$$

where A_{0-1} is Einstein's coefficient of spontaneous emission between $^5D_0$ and $^7F_1$ levels, and E_{0-J} and S_{0-J} are the energy and the integrated intensity of the $^5D_0 \rightarrow {}^7F_J$ transitions, respectively. Since the $^5D_0 \rightarrow {}^7F_1$ transition does not depend on the local ligand field, it can be used as a reference for the whole spectrum. Since *in vacuo*, $(A_{0-1})_{vac} = 14.65\ s^{-1}$,[45] if an average index of refraction n equal to 1.5 was considered, the value of $A_{0-1} = n^3A_{(0-1)vac} \approx 50\ s^{-1}$.[44,46] Using eqn (1)–(4), the parameters k_r, k_{nr}, q and n_w can be obtained, as reported in Table 3. The lower number of water molecules in Euphen-Ph-MCM-41 than in Euphen indicates an alteration of the Eu(III) first coordination shell occurring when Euphen was incorporated into MCM-41 framework, which is in agreement with the results obtained from the R values. In the meanwhile, the decrease of the non-radiative transition probability k_{nr} (around 38%) in Euphen-Ph-MCM-41 results in a longer Eu^{3+} lifetime. The decrease of k_{nr} together with the increase of k_r (around 54%) in Euphen-Ph-MCM-41 results in an increase of q by *ca.* 66%, suggesting that there is a more efficient intramolecular energy transfer process (from ligand-to-Eu(III)) in Euphen-Ph-MCM-41 than in Euphen.

The Eu^{3+} content was determined to be 74 mg g^{-1}, corresponding to 2.9 mol% of complex Euphen in the hybrid material Euphen-Ph-MCM-41. On the other hand, the $^5D_0 \rightarrow {}^7F_2$ emission intensity in Euphen-Ph-MCM-41 is *ca.* 0.28 of the pure complex Euphen obtained from the deconvolution results, which indicates that the luminescence intensity per Euphen molecule in Euphen-Ph-MCM-41 was enhanced after it was incorporated into the mesoporous channels although perhaps some pure complex molecules were adsorbed on the matrix.

Conclusions

The lanthanide complex Euphen was incorporated into mesoporous material Ph-Si(OEt)$_3$-modified MCM-41 through a template-ion exchange method. The preparation process involves two steps: the passivation of silanol groups on the external surface of as-synthesized MCM-41 with Ph-Si(OEt)$_3$ and ion-exchange of template by Euphen complex ions. The cationic surfactants removal is confirmed by FT-IR. The resultant hybrid material exhibits the characteristic emission of Eu^{3+} ions under UV irradiation with higher $^5D_0$ luminescence quantum efficiency, longer lifetime and better thermal stability than the corresponding pure complex. Moreover, there is a more efficient ligand-to-Eu(III) intramolecular energy transfer process in Euphen-Ph-MCM-41. The present method provides a convenient approach for preparation of luminescence hybrid materials containing lanthanide complex with tailored surface properties.

Acknowledgements

This work was supported by the National Natural Science Foundation of China (No. 20171043, No. 20372060); the Key National Natural Science Foundation of China (No. 20131010); the Important National Natural Science Foundation of China (No. 20490210); the "863" National Foundation for High Technology Development and Programming (No. 2002AA302105, No. 2002AA324080); the Foreign Communion & Cooperation of National Natural Science Foundation of China (No. 20340420326) and the National Basic Research Program of China ("973" Program) (No. 2006CB601103). Lianshe Fu thanks Fundação para a Ciência e Tecnologia (Portugal) for a post-doctoral grant (SFRH/BPD/5657/2001).

References

1 L. L. Hench and J. K. West, *Chem. Rev.*, 1990, **90**, 33.
2 P. Judeinstein and C. Sanchez, *J. Mater. Chem.*, 1996, **6**, 511.
3 C. Sanchez, F. Ribot, L. Rozes and B. Alonso, *Mol. Cryst. Liq. Cryst.*, 2000, **354**, 731.
4 L. D. Carlos, R. A. Sá Ferreira and V. de Zea Bermudez, in "Light Emission From Organic-Inorganic Hybrids Lacking Activator Center", in *Handbook of Organic-Inorganic Hybrid Materials and Nanocomposites*, ed. H. S. Nalwa, American Scientific Publishers, North Lewis Way, California, USA, 2003, Vol. 1, ch. 9, pp. 353–380.
5 C. Sanchez, G. J. de, A. A. Soler-Illia, F. Ribot, T. Lalot, C. R. Mayer and V. Cabuil, *Chem. Mater.*, 2001, **13**, 3061.
6 B. Lebeau and C. Sanchez, *Curr. Opin. Solid State Mater. Sci.*, 1999, **4**, 11.
7 (*a*) D. Avnir, D. Levy and R. Reisfeld, *J. Phys. Chem.*, 1984, **88**, 5956; (*b*) R. Reisfeld, T. Saraidarov, M. Pietraszkiewicz and S. Lis, *Chem. Phys. Lett.*, 2001, **349**, 266.
8 C. Sanchez, B. Lebeau, F. Chaput and J.-P. Boilot, *Adv. Mater.*, 2003, **15**, 1969.
9 R. Reisfeld, *Struct. Bond.*, 2004, **106**, 209.
10 G. F. De Sá, O. L. Malta, C. De Mello Donegá, A. M. Simas, R. L. Longo, P. A. Santa-Cruz and E. F. da Silva Jr, *Coord. Chem. Rev.*, 2000, **196**, 165.
11 N. Sabbatini, M. Guardingli and J. M. Lehn, *Coord. Chem. Rev.*, 1993, **123**, 201.
12 T. Jin, S. Tsutsumi, Y. Deguchi, K. Machida and G. Adachi, *J. Electrochem. Soc.*, 1995, **142**, L195.
13 (*a*) L. R. Matthews and E. T. Knobbe, *Chem. Mater.*, 1993, **5**, 1697; (*b*) M. Bredol, Th. Jüstel and S. Gutzov, *Opt. Mater.*, 2001, **18**, 337; (*c*) F. Embert, A. Mehdi, C. Reye and R. J. P. Corriu, *Chem. Mater.*, 2001, **13**, 4542; (*d*) A. M. Klonkowski, S. Lis, M. Pietraszkiewicz, Z. Hnatejko, K. Czarnobaj and M. Elbanowski, *Chem. Mater.*, 2003, **15**, 656.
14 (*a*) K. Binnemans, P. Lenaerts, K. Driesen and C. Görller-Walrand, *J. Mater. Chem.*, 2004, **14**, 191; (*b*) K. Driesen, P. Lenaerts, K. Binnemans and C. Görller-Walrand, *Phys. Chem. Chem. Phys.*, 2002, **4**, 552; (*c*) K. Driesen, S. Fourier, C. Görller-Walrand and K. Binnemans, *Phys. Chem. Chem. Phys.*, 2003, **5**, 198; (*d*) K. Driesen, R. Van Deun, C. Görller-Walrand and K. Binnemans, *Chem. Mater.*, 2004, **16**, 1531.
15 (*a*) G. D. Qian, M. Q. Wang, M. Wang, X. P. Fan and Z. L. Hong, *J. Mater. Sci. Lett.*, 1997, **16**, 322; (*b*) L. S. Fu, Q. G. Meng, H. J. Zhang, S. B. Wang, K. Y. Yang and J. Z. Ni, *J. Phys. Chem. Solids*, 2000, **61**, 1877.
16 (*a*) D. W. Dong, S. C. Jiang, Y. F. Men, X. L. Ji and B. Z. Jiang, *Adv. Mater.*, 2000, **12**, 646; (*b*) H. R. Li, J. Lin, H. J. Zhang, H. C. Li, L. S. Fu and Q. G. Meng, *Chem. Commun.*, 2001, 1212; (*c*) H. R. Li, J. Lin, H. J. Zhang, L. S. Fu, Q. G. Meng and S. B. Wang, *Chem. Mater.*, 2002, **14**, 3651; (*d*) A. C. Franville, D. Zambon, R. Mahiou and Y. Troin, *Chem. Mater.*, 2000, **12**, 428; (*e*) F. Y. Liu, L. S. Fu, J. Wang, Z. Liu, H. R. Li and H. J. Zhang, *Thin Solid Films*, 2002, **419**, 178; (*f*) F. Y. Liu, L. S. Fu, J. Wang, Q. G. Meng, H. R. Li, J. F. Guo and H. J. Zhang, *New J. Chem.*, 2003, **27**, 233; (*g*) H. R. Li, J. B. Yu, F. Y. Liu, H. J. Zhang, L. S. Fu, Q. G. Meng, C. Y. Peng and J. Lin, *New J. Chem.*, 2004, **28**, 1137.
17 H. H. Li, S. Inoue, K. Machida and G. Adachi, *J. Lumin.*, 2000, **87–89**, 1069.

18 H. H. Li, S. Inoue, K. Machida and G. Adachi, *Chem. Mater.*, 1999, **11**, 3171.

19 (*a*) L. D. Carlos, R. A. Sá Ferreira, J. P. Rainho and V. de Zea Bermudez, *Adv. Funct. Mater.*, 2002, **12**, 819; (*b*) V. Bekiari, G. Pistolis and P. Lianos, *Chem. Mater.*, 1999, **11**, 3189; (*c*) V. Bekiari and P. Lianos, *Adv. Mater.*, 2000, **12**, 1603; (*d*) V. Bekiari and P. Lianos, *Adv. Mater.*, 1998, **10**, 1455; (*e*) V. Bekiari, P. Lianos and P. Judeinstein, *Chem. Phys. Lett.*, 1999, **307**, 310; (*f*) R. Moleski, E. Stathatos, V. Bekiari and P. Lianos, *Thin Solid Films*, 2002, **416**, 279; (*g*) P. A. Tanner, B. Yan and H. J. Zhang, *J. Mater. Sci.*, 2000, **35**, 4325; (*h*) L. S. Fu, H. J. Zhang, S. B. Wang, Q. G. Meng, K. Y. Yang and J. Z. Ni, *J. Sol-Gel Sci. Technol.*, 1999, **15**, 49.

20 (*a*) H. Maas, A. Currao and G. Calzaferri, *Angew. Chem. Int. Ed.*, 2002, **41**, 2495; (*b*) I. L. V. Rosa, O. A. Serra and E. J. Nassar, *J. Lumin.*, 1997, **72–74**, 532.

21 Q. H. Xu, L. S. Fu, L. S. Li, H. J. Zhang and R. R. Xu, *J. Mater. Chem.*, 2000, **10**, 2532.

22 (*a*) Q. H. Xu, L. S. Li, X. S. Liu and R. R. Xu, *Chem. Mater.*, 2002, **14**, 549; (*b*) Y. F. Yao, M. S. Zhang, J. X. Shi, M. L. Gong, H. J. Zhang and Y. S. Yang, *J. Chin. Rare Earths Soc.*, 2000, **18**, 305; (*c*) L. J. Bian, H. A. Xi, X. F. Qian, J. Yin, Z. K. Zhu and Q. H. Lu, *Mater. Res. Bull.*, 2002, **14**, 2293; (*d*) Q. G. Meng, P. Boutinaud, A.-C. Franville, H. J. Zhang and R. Mahiou, *Microporous Mesoporous Mater.*, 2003, **65**, 127; (*e*) L. S. Fu, Q. H. Xu, H. J. Zhang, L. S. Li, Q. G. Meng and R. R. Xu, *Mater. Sci. Eng. B*, 2002, **88**, 68; (*f*) H. R. Li, L. S. Fu, F. Y. Liu, S. B. Wang and H. J. Zhang, *New. J. Chem.*, 2002, **26**, 674.

23 (*a*) P. C. R. Soares-Santos, H. I. S. Nogueira, V. Félix, M. G. B. Drew, R. A. Sá Ferreira, L. D. Carlos and T. Trindade, *Chem. Mater.*, 2003, **15**, 100; (*b*) L. H. Lu, F. Y. Liu, G. Y. Sun, H. J. Zhang, S. Q. Xi and H. S. Wang, *J. Mater. Chem.*, 2004, **14**, 2760.

24 P. N. Minoofar, R. Hernandez, S. Chia, B. Dunn, J. I. Zink and A. C. Franville, *J. Am. Chem. Soc.*, 2002, **124**, 14388.

25 (*a*) R. J. P. Corriu, F. Embert, Y. Guari, A. Mehdi and C. Reye, *Chem. Commun.*, 2001, 1116; (*b*) R. J. P. Corriu, A. Mehdi, C. Reye, C. Thieuleux, A. Frenkel and A. Gibaud, *New J. Chem.*, 2004, **28**, 156.

26 J. S. Beck, J. C. Vartuli, W. J. M. Roth, E. Leonowicz, C. T. Kresge, K. D. Schmitt, C. T.-W. Chu, D. H. Olson, E. W. Sheppard, S. B. McCullen, J. B. Higgins and J. L. Schlenkert, *J. Am. Chem. Soc.*, 1992, **114**, 10834.

27 B. J. Scott, G. Wirnsberger and G. D. Stucky, *Chem. Mater.*, 2001, **13**, 3140.

28 (*a*) N. Lang and A. Tuel, *Chem. Mater.*, 2004, **16**, 1961; (*b*) S. Dai, M. C. Burleigh, Y. S. Shin, C. C. Morrow, C. E. Barnes and Z. L. Xue, *Angew. Chem. Int. Ed.*, 1999, **38**, 1235.

29 (*a*) Z. T. Zhang, S. Dai, X. D. Fan, D. A. Blom, S. J. Pennycook and Y. Wei, *J. Phys. Chem. B*, 2001, **105**, 6755; (*b*) S. Dai, Y. S. Shin, Y. H. Ju, M. C. Burleigh, C. E. Barnes and Z. L. Xue, *Adv. Mater.*, 1999, **11**, 1226.

30 A.-R. Badiei and L. Bonneviot, *Inorg. Chem.*, 1998, **37**, 4142.

31 S. Z. Wang, D.-G. Choi and S.-M. Yang, *Adv. Mater.*, 2002, **14**, 1311.

32 F. De Juan and E. Ruiz-Hitzky, *Adv. Mater.*, 2000, **12**, 430.

33 F. A. Hart and F. P. Laming, *J. Inorg. Nucl. Chem.*, 1964, **26**, 579.

34 (*a*) K. S. W. Sing, D. H. Everett, R. A. W. Haul, L. Moscou, R. A. Pierotti, J. Rouquerol and T. Siemieniewska, *Pure Appl. Chem.*, 1985, **57**, 603; (*b*) S. J. Gregg and K. S. W. Sing, *Adsorption, Surface Area and Porosity*, Academic Press, London, 1982; (*c*) M. Kruk and M. Jaroniec, *Chem. Mater.*, 2001, **13**, 3169.

35 C. Y. Peng, H. J. Zhang, Q. G. Meng, H. R. Li, J. B. Yu, J. F. Guo and L. N. Sun, *Inorg. Chem. Commun.*, 2005, **8**, 440.

36 (*a*) W. Kolodziejsli, A. Corma, M. T. Navarro and J. Perez-Parientte, *Solid State Nucl. Magn. Reson.*, 1993, **2**, 253; (*b*) M. Luhmer, J. B. d'Espinose, H. Hommel and A. P. Legrand, *Magn. Reson. Imaging*, 1996, **14**, 911.

37 S. Huh, J. W. Wiench, J.-C. Yoo, M. Pruski and V. S.-Y. Lin, *Chem. Mater.*, 2003, **15**, 4247.

38 T. C. Wong, N. B. Wong and P. A. Tanner, *J. Colloid Interface Sci.*, 1997, **186**, 325.

39 (*a*) B. Julián, R. Corberán, E. Cordoncillo, P. Escribano, B. Viana and C. Sanchez, *J. Mater. Chem.*, 2004, **14**, 3337; (*b*) H. G. Zhu, D. J. Jones, J. Zajac, R. Dutartre, M. Rhomari and J. Rozière, *Chem. Mater.*, 2002, **14**, 4886.

40 A. F. Kirby, D. Foster and F. S. Richardson, *Chem. Phys. Lett.*, 1983, **95**, 507.

41 (*a*) O. L. Malta and L. D. Carlos, *Quim. Nova*, 2003, **26**, 889; (*b*) T. R. Zhang, C. Spitz, M. Antonietti and C. F. J. Faul, *Chem. Eur. J.*, 2005, **11**, 1001.

42 H. Xin, M. Shi, X. C. Gao, Y. Y. Huang, Z. L. Gong, D. B. Nie, H. Cao, Z. Q. Bian, F. Y. Li and C. H. Huang, *J. Phys. Chem. B*, 2004, **108**, 10796.

43 R. M. Supkowski and W. D. Horrocks Jr., *Inorg. Chim. Acta*, 2002, **340**, 44.

44 (*a*) L. D. Carlos, Y. Messaddeq, H. F. Brito, R. A. Sá Ferreira, V. de Zea Bermudez and S. J. L. Ribeiro, *Adv. Mater.*, 2000, **12**, 594; (*b*) R. A. Sá Ferreira, L. D. Carlos, R. R. Gonçalves, S. J. L. Ribeiro and V. de Zea Bermudez, *Chem. Mater.*, 2001, **13**, 2991.

45 M. H. V. Werts, R. T. F. Jukes and J. W. Verhoeven, *Phys. Chem. Chem. Phys.*, 2002, **4**, 1542.

46 (*a*) M. F. Hazenkamp and G. Blasse, *Chem. Mater.*, 1990, **2**, 105; (*b*) S. J. L. Ribeiro, K. Dahmouche, C. A. Ribeiro, C. V. Santilli and S. H. J. Pulcinelli, *J. Sol-Gel Sci. Technol.*, 1998, **13**, 427.